Mutations in Fibronectin Cause a Subtype of Spondylometaphyseal Dysplasia with "Corner Fractures"

Chae Syng Lee,[1] He Fu,[2] Nissan Baratang,[2] Justine Rousseau,[2] Heena Kumra,[1] V. Reid Sutton,[3] Marcello Niceta,[4] Andrea Ciolfi,[4] Guilherme Yamamoto,[5] Débora Bertola,[5] Carlo L. Marcelis,[6] Dorien Lugtenberg,[6] Andrea Bartuli,[4] Choel Kim,[7] Julie Hoover-Fong,[8] Nara Sobreira,[8] Richard Pauli,[9] Carlos Bacino,[3] Deborah Krakow,[10] Jillian Parboosingh,[11] Patrick Yap,[12] Ariana Kariminejad,[13] Marie T. McDonald,[14] Mariana I. Aracena,[15] Ekkehart Lausch,[16] Sheila Unger,[17] Andrea Superti-Furga,[17] James T. Lu,[18] Baylor-Hopkins Center for Mendelian Genomics,[19] Dan H. Cohn,[20] Marco Tartaglia,[4] Brendan H. Lee,[3] Dieter P. Reinhardt,[1,21,*] and Philippe M. Campeau[2,21,*]

Fibronectin is a master organizer of extracellular matrices (ECMs) and promotes the assembly of collagens, fibrillin-1, and other proteins. It is also known to play roles in skeletal tissues through its secretion by osteoblasts, chondrocytes, and mesenchymal cells. Spondylometaphyseal dysplasias (SMDs) comprise a diverse group of skeletal dysplasias and often manifest as short stature, growth-plate irregularities, and vertebral anomalies, such as scoliosis. By comparing the exomes of individuals with SMD with the radiographic appearance of "corner fractures" at metaphyses, we identified three individuals with fibronectin (*FN1*) variants affecting highly conserved residues. Furthermore, using matching tools and the SkelDys emailing list, we identified other individuals with *de novo FN1* variants and a similar phenotype. The severe scoliosis in most individuals and rare developmental coxa vara distinguish individuals with *FN1* mutations from those with classical Sutcliffe-type SMD. To study functional consequences of these *FN1* mutations on the protein level, we introduced three disease-associated missense variants (p.Cys87Phe [c.260G>T], p.Tyr240Asp [c.718T>G], and p.Cys260Gly [c.778T>G]) into a recombinant secreted N-terminal 70 kDa fragment (rF70K) and the full-length fibronectin (rFN). The wild-type rF70K and rFN were secreted into the culture medium, whereas all mutant proteins were either not secreted or secreted at significantly lower amounts. Immunofluorescence analysis demonstrated increased intracellular retention of the mutant proteins. In summary, *FN1* mutations that cause defective fibronectin secretion are found in SMD, and we thus provide additional evidence for a critical function of fibronectin in cartilage and bone.

Spondylometaphyseal dysplasias (SMDs), or bone dysplasias affecting the spine and growth plates, comprise a heterogeneous group of conditions from both a clinical and genetic perspective. Genetic mutations have been identified for several SMDs (in *COL2A1* [MIM: 120140], *TRPV4* [MIM: 605427], *SBDS* [MIM: 607444], *GPX4* [MIM: 138322], *PCYT1A* [MIM: 123695], and *ACP5* [MIM: 171640]), but rarer forms still escape molecular diagnosis.[1] One such condition is SMD with "corner fractures" (MIM: 184255). First recognized by Sutcliffe in 1966, fewer than 25 individuals or families have been reported.[2] These individuals generally show developmental coxa vara but no scoliosis (as was the case for several individuals in our cohort without *FN1* [MIM: 135600] mutations; see Table S1).[3,4] At the edges of the irregular metaphyses, flake-like, triangular, or curvilinear ossification centers simulate fractures. This specifically affects the distal tibia, the distal radius (ulnar aspect), the proximal humerus, and the proximal femur. The so-called "corner fractures" are unlikely to be true fractures but instead represent irregular ossification at the growth plates and secondary ossification centers.[3] These fractures tend to become larger in older children and disappear after growth has stopped. Corner fractures on radiographs can also be seen in Duetting-type SMD (or SMD type A4 [MIM: 609052]),[5] Schmid (MIM: 156500) and Jansen (MIM: 156400) types of metaphyseal chondrodysplasia, Strudwick-type spondyloepimetaphyseal dysplasia (MIM: 184250),[6] Blount disease

[1]Department of Anatomy and Cell Biology and Faculty of Dentistry, McGill University, Montreal, QC H3A 0C7, Canada; [2]Centre Hospitalier Universitaire Sainte Justine Research Centre, University of Montreal, Montreal, QC H3T 1C5, Canada; [3]Department of Molecular and Human Genetics, Baylor College of Medicine, Houston, TX 77030, USA; [4]Genetics and Rare Diseases Research Division, Bambino Gesù Children's Hospital, Istituto di Ricovero e Cura a Carattere Scientifico, Rome 00146, Italy; [5]Clinical Genetics Unit, Instituto da Criança, Hospital das Clínicas da Faculdade de Medicina da Universidade de São Paulo, São Paulo SP 05403-000, Brazil; [6]Department of Human Genetics, Radboud University Medical Center, 6500 HB Nijmegen, the Netherlands; [7]Department of Pharmacology, Baylor College of Medicine, Houston, TX 77030, USA; [8]McKusick-Nathans Institute of Genetic Medicine, Johns Hopkins University School of Medicine, Baltimore, MD 21287, USA; [9]Midwest Regional Bone Dysplasia Clinic, University of Wisconsin, Madison, WI 53705, USA; [10]Department of Human Genetics, David Geffen School of Medicine, University of California, Los Angeles, Los Angeles, CA 90095, USA; [11]Department of Medical Genetics and Alberta Children's Hospital Research Institute, University of Calgary, Calgary, AB T2N 4N1, Canada; [12]Genetic Health Service New Zealand (Northern Hub), Auckland 1023, New Zealand; [13]Kariminejad-Najmabadi Pathology & Genetics Center, Tehran 14665, Iran; [14]Department of Pediatrics, Division of Medical Genetics, Duke University Medical Center, Durham, NC 27710, USA; [15]División de Pediatría, Pontificia Universidad Católica de Chile, Pediatra-Genetista, Unidad de Genética, Hospital Dr. Luis Calvo Mackenna, Santiago, Chile; [16]Department of Pediatrics, Medical Center, Faculty of Medicine, University of Freiburg, Freiburg 79106, Germany; [17]Service of Medical Genetics, Lausanne University Hospital (CHUV), Lausanne 1011, Switzerland; [18]Helix, San Carlos, CA 94070, USA; [19]Baylor-Hopkins Center for Mendelian Genomics, Houston, TX 77030, USA; [20]Department of Molecular, Cell, and Developmental Biology, University of California, Los Angeles, Los Angeles, CA 90095, USA
[21]These authors contributed equally to this work
*Correspondence: dieter.reinhardt@mcgill.ca (D.P.R.), p.campeau@umontreal.ca (P.M.C.)
https://doi.org/10.1016/j.ajhg.2017.09.019.

Table 1. Clinical Features

	Family 1			Family 2	Family 3	Family 4	Family 5	Family 6	Family 7	SMD Corner-Fracture Type or Sutcliffe Type (from Currarino et al.;[3] n = 18)
Individual in pedigree	II-2 (mother)	III-1 (first child)	III-2 (second child)	II-1	II-1	III-2 (child)	II-1	II-1	II-1	NA
Gender	female	male	male	male	female	female	female	female	female	NA
Age at last assessment	29 years	13 years	9 years	14 years	3 years, 9 months	2 years, 1 month	5 years, 9 months	16 years, 11 months	4 years	NA
Height (cm)	147 (−3 SD)	113 (−5.7 SD)	107 (−4.6 SD)	136 (−3.38 SD)	92 (−2.5 SD)	83.7 (−0.9 SD)	97 (−3.3 SD)	137 (−4.66 SD)	89 (<3.0 SD)	NA
Ovoid vertebral bodies	NA	+	−	−	+	−	+	+	+	16/18
Scoliosis	+ (operated)	+ (operated)	+ (operated)	+	−	−	+ (operated)	+	+	1/18
Developmental coxa vara	−	−	−	−	−	+	−	+	+	18/18
Irregular metaphyses	NA	+	+	+	+	+	+	+	+	16/18
"Corner fractures"	−	+	+	+	+	+	+	+	+	15/18
Knee anomalies	−	−	genu varum (operated)	−	genu varum	−	genu varum (operated)	−	genu varum	one genu varum, one genum valgum
Chest or rib anomaly (e.g., pectus)	pectus carinatum	pectus carinatum	pectus carinatum	−	NA	−	pectus carinatum	−	−	NA
Other	hip surgery at 18 years, pregnancy-induced hypertension	born at term, weight 1,673 g (−4.3 SD), length 38 cm (−2.7 SD), hyponatremia at 1 month (unknown cause), hypoplasia of T12 vertebra and triangular S1, back and leg pain	born at term, weight 1,729 g (−3.9 SD), length 39 cm (−2.6 SD), leg pain	facial asymmetry and dysmorphisms (dysplastic left ear), missing teeth 34 and 44 (island of compact bone instead), intradural lipoma and megacisterna magna on MRI	born at 33 weeks, weight 1,754 g	femoral rodding	born at 36 weeks, weight 2,060 g (3^{rd}–10^{th} percentile), length 43.5 cm (3^{rd}–10^{th} percentile), OFC 29.5 cm (3^{rd} percentile), normal renal sonography and kidney function, no signs of proteinuria or microalbuminuria, leg pain	born at 39 weeks, weight 2,280 g (<3^{rd} percentile), length 45 cm (<3^{rd} percentile), OFC 32 (3^{rd} percentile), hip surgery at 2 years (both sides), multiple corrections to right hip and femur, shortening of right leg by 5 cm, bicuspid aortic valve	normal renal function, no proteinuria, no facial asymmetry or dysmorphisms	NA

The following abbreviations are used: OFC, occipitofrontal circumference; and NA, not available.

Table 2. Genetic Description of the *FN1* Variants

Family	Genomic Change (hg19)	Coding Change (GenBank: NM_212482.2)[a]	Protein Change (GenBank: NP_997647.1)	Inheritance
1	chr2: g.216299436C>A	c.260G>T	p.Cys87Phe	dominant
2	chr2: g.216298095A>G	c.367T>C	p.Cys123Arg	*de novo*
3	chr2: g.216295448G>C	c.675C>G	p.Cys225Trp	*de novo*
4	chr2: g.216293029A>C	c.718T>G	p.Tyr240Asp	dominant
5	chr2: g.216292969A>C	c.778T>G	p.Cys260Gly	*de novo*
6	chr2: g.216273022_216273024del	c.2425_2427del	p.Thr809del	*de novo*
7	chr2: g.216298095A>G	c.367T>C	p.Cys123Arg	*de novo*

[a]All variants are absent from the ExAC Browser.

(MIM: 188700), Menkes disease (MIM: 309400), nonaccidental injury, congenital contractures, rickets, and scurvy.[7] Some individuals initially thought to have SMD with corner fractures were later identified to have type 2 collagenopathy.[6]

Fibronectin is found in the human body in both a soluble form (~300 μg/mL in plasma) and an insoluble form as a principal component of the fibrillar extracellular matrix (ECM) of virtually all tissues.[8,9] Fibronectin contains binding sites for integrins, collagens,

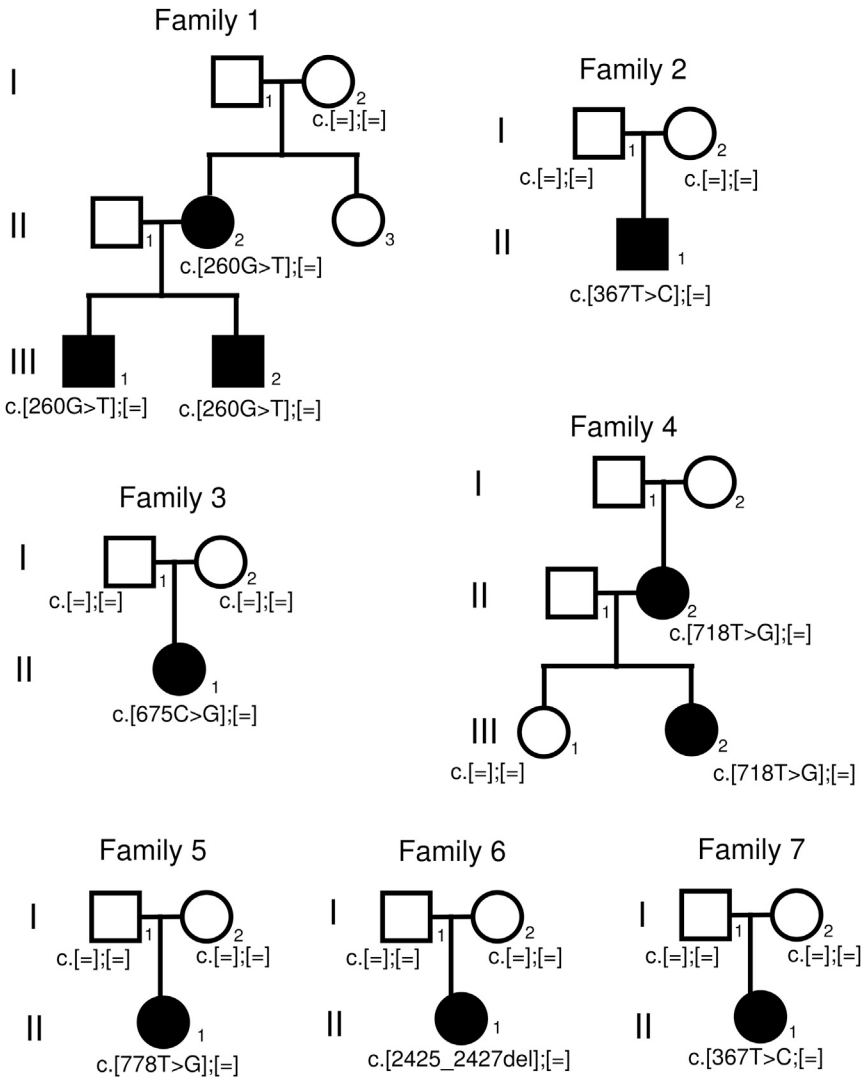

Figure 1. Pedigrees of the Families with *FN1* Mutations
Co-segregation of the variants with the trait in families 1 and 4 suggests dominant inheritance. Consistently, *de novo FN1* mutations in the affected individuals of simplex families 2, 3, 5, 6, and 7 were observed.

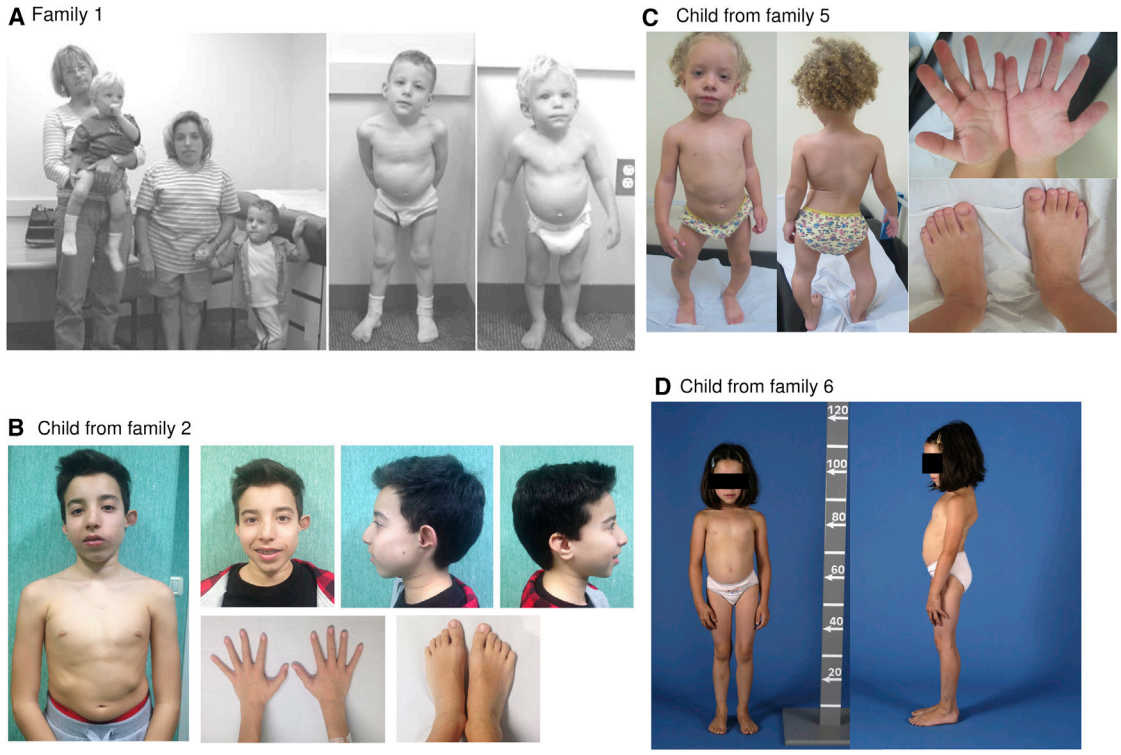

Figure 2. Photographs of Some of the Individuals with *FN1* Mutations
(A) Photographs in a figure reproduced with permission from Sutton et al.[30] (copyright © 2005 Wiley-Liss, Inc.). On the left are the three affected individuals who have an *FN1* mutation and the maternal grandmother. In the middle is the older child at age 5 years, and on the right is the younger child at age 3 years.
(B) Affected child from family 2 at age 13 years. Note the short trunk, facial asymmetry, dysplastic left ear, and normal hands and feet.
(C) Affected child from family 5 at age 2 years and 11 months. Note the scoliosis, genu varum, and normal hands and feet.
(D) Affected child from family 6 at age 8 years. Note the short trunk and scoliotic posture.

glycoproteins, and glycosaminoglycans, as well as self-association sites.[10] It self-assembles in a cell-dependent manner upon binding to integrins and other cell-surface components[9] and initiates the assembly of the ECM.[11–13]

We performed exome sequencing in individuals with SMD with corner fractures, who had been identified through the Texas Children's Skeletal Dysplasia Program, International Skeletal Dysplasia Registry, Baylor-Hopkins Center for Mendelian Genetics, Skeldys emailing list of the International Skeletal Dysplasia Society (ISDS), Shriners Canada Skeletal Dysplasia Clinic, and existing collaborations. Families provided written informed consent for protocols approved by the institutional review board at Baylor College of Medicine or local institutions. The procedures followed were in accordance with the ethical standards of the relevant committees on human experimentation. Details on the exome sequencing libraries and alignment are presented in Table S2.

In two of the first few individuals sequenced, who have been previously reported, *COL2A1* mutations were identified.[1] In total, 13 individuals were exome sequenced, and a comparison of the rare or undescribed variants shared between these individuals revealed variants in *FN1* in three of these affected individuals (two variants segregating with the disease, c.260G>T [p.Cys87Phe] [GenBank: NM_212482.2 and NP_997647.1, respectively] in family 1 and c.718T>G [p.Tyr240Asp] in family 4, and a *de novo* variant, c.2425_2427del [p.Thr809del] in family 6). The genetic cause of SMD is still undetermined for the other individuals. Subsequently, through the ISDS emailing list, the GeneMatcher tool, and the Shriners Canada Skeletal Dysplasia Clinic,[14] four other individuals with *de novo FN1* variants (c.367T>C [p.Cys123Arg] in families 2 and 7, c.675C>G [p.Cys225Trp] in family 3, and c.778T>G [p.Cys260Gly] in family 5) and SMD with corner fractures were identified. In one of them (individual 3, identified with the ISDS emailing list), only *FN1* was sequenced on the basis of the initial findings. Thus, in this cohort, previously unreported *FN1* variants were found in 7 of 16 families affected by SMD with corner fractures. The clinical phenotypes of the individuals with *FN1* variants are detailed in Table 1, and the variants are presented in Table 2. Figure 1 shows pedigrees, Figure 2 shows photographs, Figure 3 shows selected radiographs, and Figure S1 shows additional radiographs.

All *FN1* variants discovered in this study are absent from the ExAC Browser and affect highly conserved residues

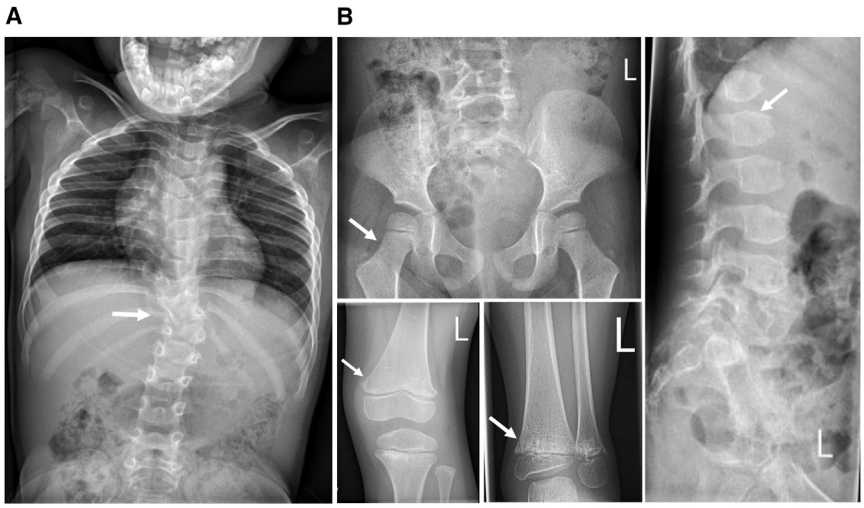

Figure 3. Radiographs Showing the "Corner Fractures" and Other Radiological Changes
(A) Individual from family 7; note the significant scoliosis.
(B) Individual from family 3; note the absence of coxa vara, the presence of irregular metaphyses with corner fractures, and the presence of ovoid vertebral bodies.
Additional radiographs from all families are available in Figure S1.

(Figure 4). The majority (4/6) affect cysteine residues, all of which form disulfide bonds that are critical for the three-dimensional structure of the type I fibronectin domains.[15] Five of the mutations (c.260G>T [p.Cys87Phe], c.367T>C [p.Cys123Arg], c.675C>G [p.Cys225Trp], c.718T>G [p.Tyr240Asp], and c.778T>G [p.Cys260Gly]) are located in the N-terminal assembly domain (spanning fibronectin domains I-1 through I-5), which is important to initiating assembly on the cell surface.[9] The remaining mutation (c.2425_2427del [p.Thr809del]) was found in the III-2 domain, which contains a fibronectin binding site and is involved in conformational changes promoting fibronectin assembly.[9] The Tyr240 residue has previously been mutated into a Ser residue *in vitro* and shown to be critical for fibronectin binding to fibroblasts.[16]

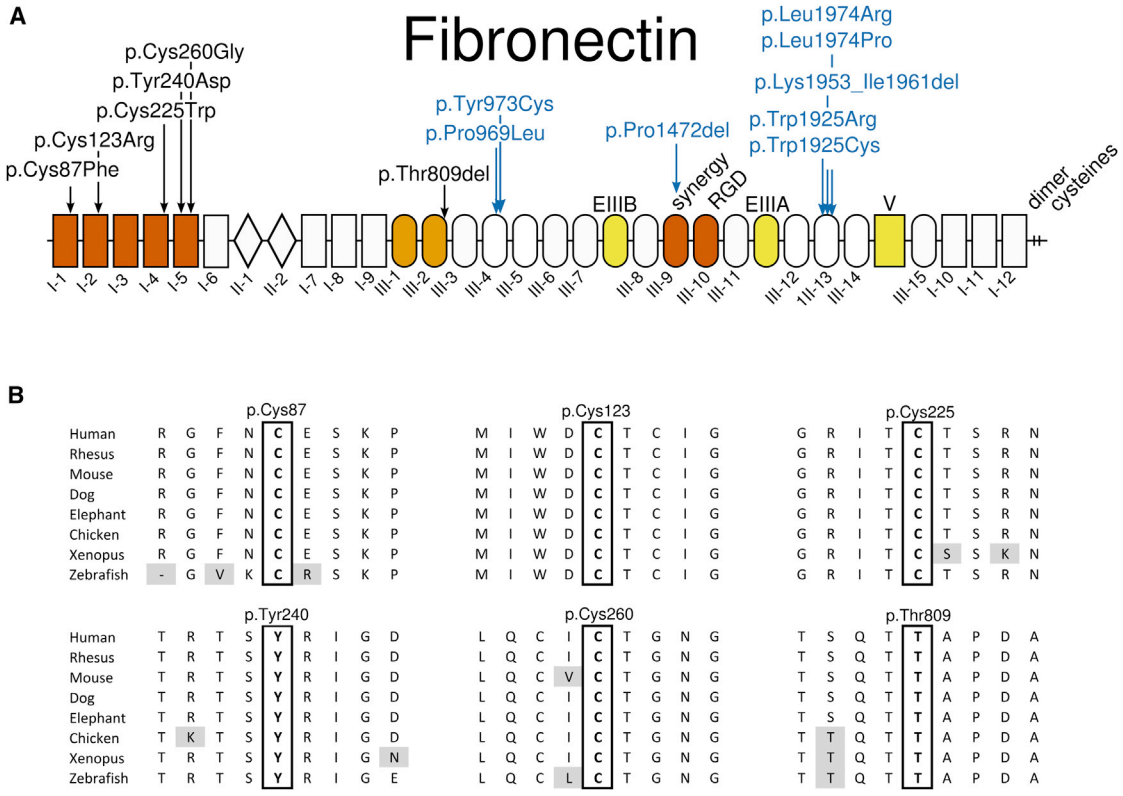

Figure 4. Position and Conservation of Amino Acids Affected by Substitutions
(A) Location of the SMD-associated fibronectin amino acid substitutions (in black) and those underlying glomerulopathy (in blue). The fibronectin domains I, II, and III are numbered, V stands for variable domain, and EIIIA and EIIIB indicate the extra type III repeat A and B segments. These three domains in yellow are subject to alternative splicing. Domains I-1 to I-5 in red represent the N-terminal assembly domain. Domains III-9 and III-10, also in red, contain the synergy site and the RGD site. Domains III-1 and III-2, in orange, contain self-interaction sites and are involved in conformational changes promoting fibronectin assembly.
(B) Amino acid conservation of the mutated residues across vertebrates. Gray shading indicates non-conserved amino acid residues.

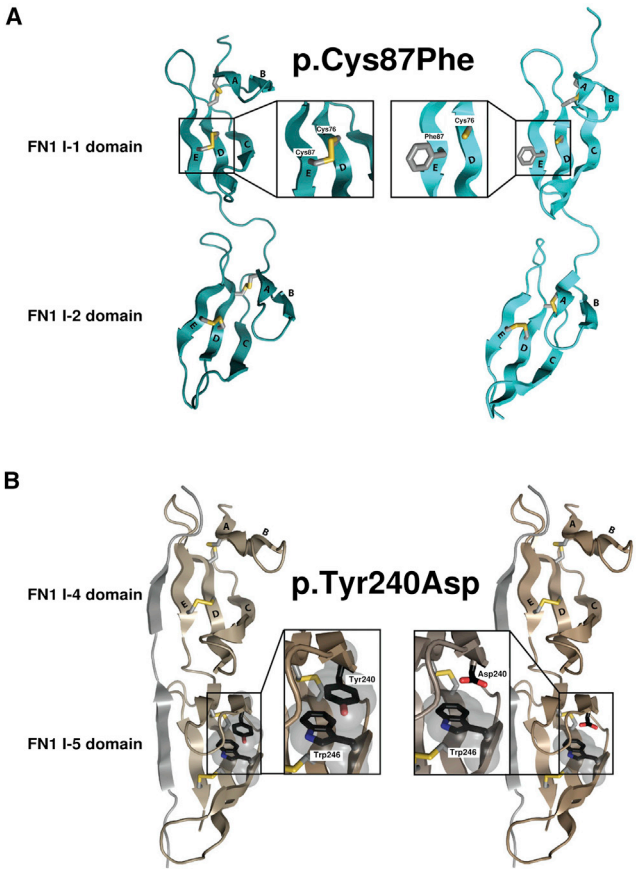

Figure 5. Structural Impact of SMD-Causing Mutations
(A) Structural models of fibronectin domains I-1 and I-2 (PDB: 1O9A,[31] without the *S. dysgalactiae* FnBP B3 peptide). On the left is the wild-type protein, and on the right is the model with the variant. The model for the p.Cys87Phe substitution was generated by the ModWeb Server.[32] The disulfide bond formed between Cys76 and Cys87 stabilizes domain I-1. The p.Cys87Phe substitution is predicted to destabilize the structure by breaking the disulfide bond and by displaying a hydrophobic residue at the surface.
(B) Structural models of fibronectin domains I-4 and I-5 (PDB: 2RKY,[33] without the *S. aureus* FnBPA peptide). To generate the model for the p.Tyr240Asp change, we replaced tyrosine with aspartic acid and manually adjusted the rotomer position to minimize the steric clash with the rest of the protein by using Coot.[34] For the wild-type protein, the side chains of Tyr240 and Trp246 interact through π stacking and stabilize the fibronectin domain. This interaction is predicted to be lost in the mutant protein.

Heterozygous *FN1* mutations have previously been reported in type 2 autosomal-dominant glomerulopathy with fibronectin deposits (MIM: 601894).[17] Remarkably, all *FN1* mutations previously implicated in this glomerulopathy cluster in more C-terminally-located regions important for heparin binding and integrin binding (Figure 4).[17–19] *In vitro*, the mutations cause decreased heparin and integrin binding, reduced endothelial cell spreading, and cytoskeletal reorganization, which has been hypothesized to affect glomerular size selectivity and protein trafficking. Importantly, none of the SMD individuals in our cohort had any evidence of renal disease.

As stated above, all cysteine residues affected by mutations in our cohort are involved in disulfide bonds in fibronectin type I domains (bridges form between Cys87 and Cys76, between Cys123 and Cys135, between Cys225 and Cys213, and between Cys260 and Cys231). We selected one of these (p.Cys87Phe) to model the consequence of the mutation on the three-dimensional structure of fibronectin domains (Figure 5A). The p.Cys87Phe substitution was predicted to destabilize the structure of the I-1 domain by breaking the disulfide bond with residue Cys76 and by displaying a hydrophobic residue at the surface. A similar disruptive impact was predicted for the other missense changes involving Cys123, Cys225, and Cys260. For the two other amino acid residues affected by mutations (Tyr240 and Thr809), 3D structures adequate for modeling the mutations were available only for p.Tyr240Asp (Thr809 was found only at the C-terminal end of a solution structure of III-2,[20] which limits the interpretation of its interactions). Modeling predicted that the p.Tyr240Asp variant would disrupt the pi-stacking (or π-π stacking) of the side chains of Tyr240 and Trp246 and thus destabilize the I-5 domain (Figure 5B).

We next aimed to analyze the functional consequences of selected *FN1* mutations on the fibronectin protein. Because cells from affected individuals were not available for this study, we generated a recombinant 70 kDa N-terminal fragment of fibronectin (rF70K), spanning the region where five of the six missense variants identified in this study are located, and a full-length recombinant fibronectin (rFN) (Figure 6A). Expression vectors for the human wild-type rF70K and rFN, as well as selected mutants, were generated by standard cloning procedures in the pcDNA3.1+ plasmid (Thermo Fisher Scientific, V79020) with the sequence for a C-terminal V5 epitope tag to facilitate detection and a hexahistidine tag intended for chromatographic purification. At the 5′ ends, the vectors contained the coding sequence for either the BM40 signal peptide (rF70K) or the native fibronectin signal peptide (rFN) to ensure secretion of the recombinant protein through the secretory pathway. The rFN expression plasmid was constructed with the sequence for the alternatively spliced EDA and EDB domains. For this analysis, we selected two cysteine missense variants (p.Cys87Phe and p.Cys260Gly) because they represent the major group of the identified mutations, as well as a non-cysteine missense variant (p.Tyr240Asp). These point mutants were generated from the wild-type plasmids via the QuikChange Site-Directed Mutagenesis Kit (Agilent Technologies, 200519).

The plasmids were transfected into human HEK293 cells, which synthesize and secrete endogenous fibronectin and represent an efficient system for producing a range of correctly folded and posttranslationally modified ECM proteins (subfragments as well as mutants).[21–23] After the plasmids were stably transfected into human HEK293 cells as described previously,[24] the secreted wild-type recombinant proteins were readily identified in the

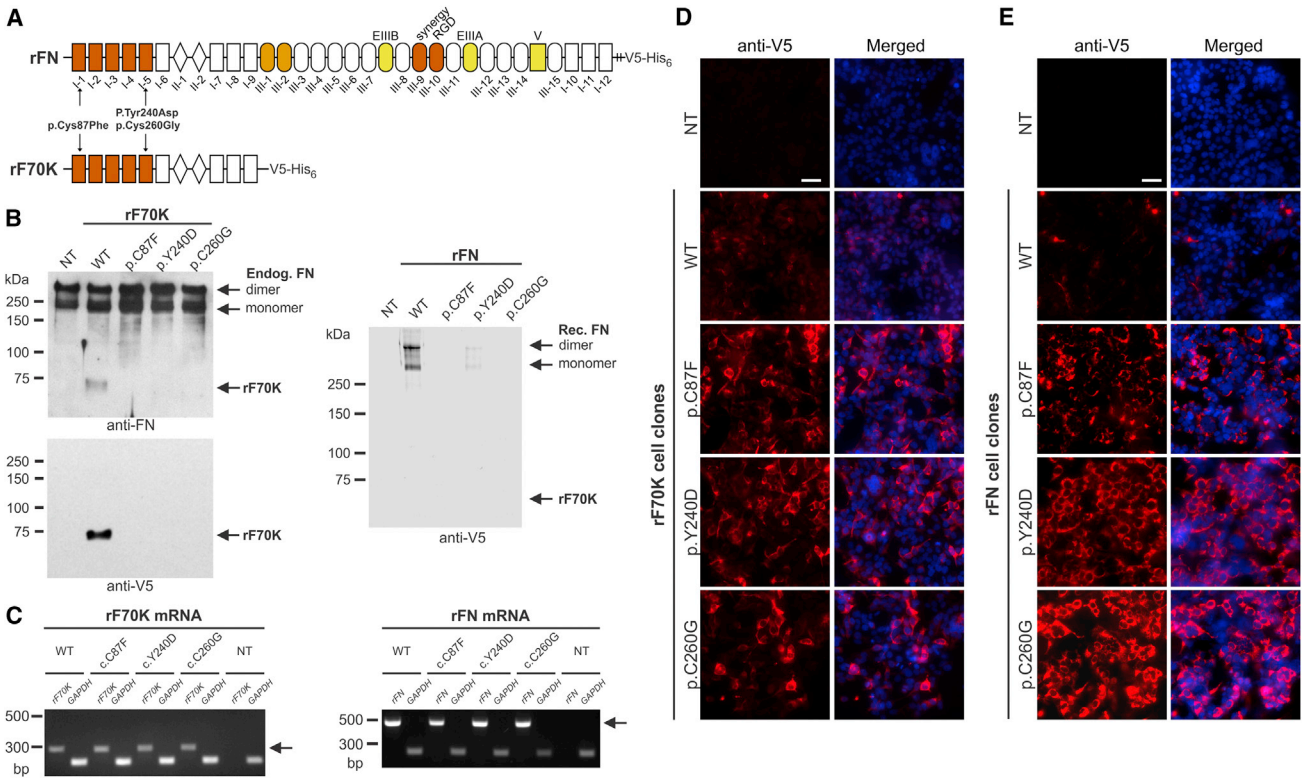

Figure 6. Analysis of Protein Secretion of Recombinant Wild-Type and SMD-Causing Mutants of rF70K and rFN

(A) Schematic overview of full-length fibronectin (rFN) and the 70 kDa N-terminal fragment of fibronectin (rF70K). To ensure secretion through the secretory pathway, the expression plasmids contain either the sequence coding for the endogenous fibronectin signal peptide (rFN) or a heterologous BM40 signal peptide (rF70K). The indicated SMD variants were engineered into the expression constructs. (B–E) NT refers to the non-transfected HEK293 controls, WT refers to the wild-type rF70K or rFN cell clones, and the mutant cell clones are indicated in the one-letter amino acid code. (B) Western blot analysis of conditioned cell-culture medium (for 2 days) harvested from HEK293 cells transfected with rF70K (left) and rFN (right). Analysis of rF70K was performed with a rabbit anti-fibronectin antibody (top; primary antibody, Sigma, F3648; secondary goat anti-rabbit horseradish-conjugated antibody, Agilent Technologies, K4008) and a horseradish-conjugated anti-V5 monoclonal antibody (bottom, Thermo Fisher Scientific, MA5-15253-HRP), whereas the rFN analysis was performed with only an anti-V5 antibody, given that the anti-fibronectin antibody also reacts with endogenous fibronectin. All samples were analyzed under reducing conditions, the blots for rF70K were developed with the SuperSignal West Pico Chemiluminescent Substrate (Thermo Fisher Scientific, 34080), and the blots for rFN were developed with 0.5 mg/mL 4-chloro-1-naphthol (Sigma, C8890) in Tris-buffered saline including 0.02% H_2O_2. (C) Specific RT-PCR analysis of mRNA coding for rF70K (left; 285 bp) or rFN (right; 440 bp) (excluding the endogenous *FN1* mRNA). *GAPDH* analysis (226 bp) was included as a control. RNA was extracted with the RNeasy Plus Mini Kit (QIAGEN, 74134) according to the manufacturer's protocol. Reverse transcription was performed with the ProtoScript II First Strand cDNA Synthesis Kit (New England Biolabs, E6560S), and PCR was performed for 40 cycles. (D and E) Immunofluorescence analysis of transfected HEK293 cells 3 days after seeding with anti-V5 antibodies (red; primary antibody, Thermo Fisher Scientific, R960-25; secondary antibody, Cy3-conjugated antibody, Thermo Fisher Scientific, A10521) for rF70K and rFN was performed according to a previously established protocol.[35] Cells were fixed with 4% paraformaldehyde and permeabilized with 0.5% Triton X-100; nuclei were counter-stained with DAPI (blue). The experiments were confirmed with three to four individual recombinant cell clones. The scale bar indicates 50 μm. Images were taken at 400× magnification with Zen software and an AxioImager M2 microscope (Zeiss) equipped with an ORCA-flash 4.0 camera (Hamamatsu, C11440). Note that all analyzed rF70K and rFN mutant proteins were retained intracellularly, but the wild-type proteins were not.

cell-culture medium (conditioned for 2 days) with fibronectin-specific or anti-V5-specific antibodies (Figure 6B). Surprisingly, all three rF70K and rFN mutants were either undetectable in the culture medium or detectable at much lower levels than the wild-type protein. Analysis of recombinant mRNA with primers excluding the endogenous fibronectin mRNA revealed that the amount of mutant mRNA was similar to that of wild-type mRNA (Figure 6C). Immunofluorescence analysis demonstrated very low amounts of the wild-type proteins within the stably transfected cells because the proteins secreted into the culture medium (Figures 6D and 6E). In contrast to this finding, all three rF70K and rFN mutants consistently showed strong accumulation within the cells. These data clearly demonstrate that p.Cys87Phe, p.Tyr240Asp, and p.Cys260Gly exert a common molecular defect in fibronectin secretion. To assess whether the intracellular retention induced the unfolded protein response in HEK293 cells, we analyzed *XBP1* splicing (IRE1 pathway) and the mRNA expression levels of *CHOP* and *ATF4* (PERK pathway). However, no indication of increased *XBP1* splicing or changes in the *CHOP* or *ATF4* mRNA expression

levels was detected (Figure S2). In addition, the mutant rFN cell clones did not undergo caspase-3-mediated apoptosis (Figure S3).

Fibronectin is present throughout cartilage differentiation and persists in mature cartilaginous tissue.[25] However, little is known about the functional role of fibronectin in the development and homeostasis of cartilage. Given that fibronectin has been established as a key ECM protein that guides fibrillogenesis of several other ECM proteins, including proteins present in cartilage, such as fibrillin-1,[26] it is conceivable that a reduced amount of secreted fibronectin from chondrocytes could result in a deficient matrix network in cartilage. It is well known that mutations affecting another cartilage protein, cartilage oligomeric matrix protein (*COMP* [MIM: 600310]), lead to pseudoachondroplasia (MIM: 177170) and multiple epiphyseal dysplasia (MIM: 132400) through accumulation of mutant COMP in the endoplasmic reticulum of chondrocytes.[27] It is thought that this protein accumulation impairs secretion of other matrix proteins and leads to abnormal ECM and chondrocyte death.[28,29] It is possible that a similar mechanism exists for retained mutant fibronectin and leads to the SMD phenotype observed in our cohort. Conditional double-knockout experiments of fibronectin in mouse cartilage and liver or knockin of some of the mutations are currently underway to further elucidate the molecular basis of fibronectin in the development and maintenance of cartilage.

Accession Numbers

The accession numbers for the variants identified in this study are ClinVar: SCV000574553–SCV000574558.

Supplemental Data

Supplemental Data include three figures and two tables and can be found with this article online at https://doi.org/10.1016/j.ajhg.2017.09.019.

Acknowledgments

This project was supported in part by operating grants from the Canadian Institutes for Health Research (clinician-scientist award RN315908 to P.M.C.; MOP-137091 to D.P.R.), the Fonds de Recherche du Québec - Santé clinical research scholar award 30647 to P.M.C., the Quebec Network for Oral and Bone Health Research (RSBO Emerging Collaborating Project 2014-2015 to P.M.C. and D.P.R.), the NIH (UM1 HG006542 to the Baylor Hopkins Center for Mendelian Genomics), the Heart and Stroke Foundation of Canada (G-16-00014634 to D.P.R.), the Italian Ministry of Health (Ricerca Corrente 2016 to M.T. and M.N.), and Fondazione Bambino Gesù (Vite Coraggiose grant to M.T.). This work was also supported by NIH P01 HD070394, by HD024064 from the Eunice Kennedy Shriver National Institute of Child Health & Human Development granted to the Baylor College of Medicine (BCM) Intellectual and Developmental Disabilities Research Center (for processing samples obtained and managing clinical protocols), by the BCM Advanced Technology Cores through funding from the NIH (AI036211, CA125123, and RR024574), by the Rolanette and Berdon Lawrence Bone Disease Program of Texas, and by the BCM Center for Skeletal Medicine and Biology (to B.H.L). Analysis of individual 5 was supported by the São Paulo Research Foundation (FAPESP 2015/21783-9; Centros de Pesquisa, Inovação, e Difusão [CEPID] 2013/08028-1) and National Council for Scientific and Technological Development (CNPq 302605/2013-4 and 304130/2016-8 to D. B). E.L. is supported by grants from the German Research Foundation (CRC 1140), the German Ministry for Education and Research (MaTrOC), and the European Union (SYBIL grant agreement no. 602300; RARENET). We thank Dr. Deane Mosher and Dr. Douglas Annis for providing the FN1 pAcGP67A plasmid. We thank Dr. Reggie Hamdy for referring individual 7 to Dr. Campeau and Dr. Amélie Damphousse for the interpretation of the radiographs.

Received: April 24, 2017
Accepted: September 12, 2017
Published: November 2, 2017

Web Resources

Baylor-Hopkins Center for Mendelian Genetics (BH-CMG), http://bhcmg.org/
ExAC Browser, http://exac.broadinstitute.org/
GenBank, http://www.ncbi.nlm.nih.gov/genbank/
GeneMatcher, https://www.genematcher.org
International Skeletal Dysplasia Society (ISDS), http://www.isds.ch/
International Skeletal Dysplasia Registry (ISDR), http://ortho.ucla.edu/isdr
OMIM, http://www.omim.org/
RCSB Protein Data Bank, https://www.rcsb.org/pdb/home/home.do
UniProt, http://www.uniprot.org/uniprot/

References

1. Machol, K., Jain, M., Almannai, M., Orand, T., Lu, J.T., Tran, A., Chen, Y., Schlesinger, A., Gibbs, R., Bonafe, L., et al. (2017). Corner fracture type spondylometaphyseal dysplasia: Overlap with type II collagenopathies. Am. J. Med. Genet. A. *173*, 733–739.
2. Sutcliffe, J. (1966). Metaphyseal dysostosis. Ann. Radiol. (Paris) *9*, R215–R223.
3. Currarino, G., Birch, J.G., and Herring, J.A. (2000). Developmental coxa vara associated with spondylometaphyseal dysplasia (DCV/SMD): "SMD-corner fracture type" (DCV/SMD-CF) demonstrated in most reported cases. Pediatr. Radiol. *30*, 14–24.
4. Langer, L.O., Jr., Brill, P.W., Ozonoff, M.B., Pauli, R.M., Wilson, W.G., Alford, B.A., Pavlov, H., and Drake, D.G. (1990). Spondylometaphyseal dysplasia, corner fracture type: a heritable condition associated with coxa vara. Radiology *175*, 761–766.
5. Duetting, T., Schulze, A., Troeger, J., and Spranger, J. (1998). A rare form of spondylometaphyseal dysplasia-type A4. Am. J. Med. Genet. *78*, 61–66.
6. Walter, K., Tansek, M., Tobias, E.S., Ikegawa, S., Coucke, P., Hyland, J., Mortier, G., Iwaya, T., Nishimura, G., Superti-Furga, A., and Unger, S. (2007). COL2A1-related skeletal dysplasias with predominant metaphyseal involvement. Am. J. Med. Genet. A. *143A*, 161–167.
7. Kozlowski, K., and Beighton, P. (1984). Gamut index of skeletal dysplasias: an aid to radiodiagnosis (Springer-Verlag).

8. Mosher, D.F. (2006). Plasma fibronectin concentration: a risk factor for arterial thrombosis? Arterioscler. Thromb. Vasc. Biol. *26*, 1193–1195.
9. Singh, P., Carraher, C., and Schwarzbauer, J.E. (2010). Assembly of fibronectin extracellular matrix. Annu. Rev. Cell Dev. Biol. *26*, 397–419.
10. Pankov, R., and Yamada, K.M. (2002). Fibronectin at a glance. J. Cell Sci. *115*, 3861–3863.
11. Sabatier, L., Chen, D., Fagotto-Kaufmann, C., Hubmacher, D., McKee, M.D., Annis, D.S., Mosher, D.F., and Reinhardt, D.P. (2009). Fibrillin assembly requires fibronectin. Mol. Biol. Cell *20*, 846–858.
12. Sottile, J., and Hocking, D.C. (2002). Fibronectin polymerization regulates the composition and stability of extracellular matrix fibrils and cell-matrix adhesions. Mol. Biol. Cell *13*, 3546–3559.
13. Dallas, S.L., Sivakumar, P., Jones, C.J., Chen, Q., Peters, D.M., Mosher, D.F., Humphries, M.J., and Kielty, C.M. (2005). Fibronectin regulates latent transforming growth factor-beta (TGF beta) by controlling matrix assembly of latent TGF beta-binding protein-1. J. Biol. Chem. *280*, 18871–18880.
14. Sobreira, N., Schiettecatte, F., Valle, D., and Hamosh, A. (2015). GeneMatcher: a matching tool for connecting investigators with an interest in the same gene. Hum. Mutat. *36*, 928–930.
15. Baron, M., Norman, D., Willis, A., and Campbell, I.D. (1990). Structure of the fibronectin type 1 module. Nature *345*, 642–646.
16. Sottile, J., Schwarzbauer, J., Selegue, J., and Mosher, D.F. (1991). Five type I modules of fibronectin form a functional unit that binds to fibroblasts and Staphylococcus aureus. J. Biol. Chem. *266*, 12840–12843.
17. Ohtsubo, H., Okada, T., Nozu, K., Takaoka, Y., Shono, A., Asanuma, K., Zhang, L., Nakanishi, K., Taniguchi-Ikeda, M., Kaito, H., et al. (2016). Identification of mutations in FN1 leading to glomerulopathy with fibronectin deposits. Pediatr. Nephrol. *31*, 1459–1467.
18. Castelletti, F., Donadelli, R., Banterla, F., Hildebrandt, F., Zipfel, P.F., Bresin, E., Otto, E., Skerka, C., Renieri, A., Todeschini, M., et al. (2008). Mutations in FN1 cause glomerulopathy with fibronectin deposits. Proc. Natl. Acad. Sci. USA *105*, 2538–2543.
19. Ertoy Baydar, D., Kutlugun, A.A., Bresin, E., and Piras, R. (2013). A case of familial glomerulopathy with fibronectin deposits caused by the Y973C mutation in fibronectin. Am. J. Kidney Dis. *61*, 514–518.
20. Vakonakis, I., Staunton, D., Rooney, L.M., and Campbell, I.D. (2007). Interdomain association in fibronectin: insight into cryptic sites and fibrillogenesis. EMBO J. *26*, 2575–2583.
21. Kirschner, R., Hubmacher, D., Iyengar, G., Kaur, J., Fagotto-Kaufmann, C., Brömme, D., Bartels, R., and Reinhardt, D.P. (2011). Classical and neonatal Marfan syndrome mutations in fibrillin-1 cause differential protease susceptibilities and protein function. J. Biol. Chem. *286*, 32810–32823.
22. McKee, K.K., Harrison, D., Capizzi, S., and Yurchenco, P.D. (2007). Role of laminin terminal globular domains in basement membrane assembly. J. Biol. Chem. *282*, 21437–21447.
23. Fox, J.W., Mayer, U., Nischt, R., Aumailley, M., Reinhardt, D., Wiedemann, H., Mann, K., Timpl, R., Krieg, T., Engel, J., et al. (1991). Recombinant nidogen consists of three globular domains and mediates binding of laminin to collagen type IV. EMBO J. *10*, 3137–3146.
24. Lin, G., Tiedemann, K., Vollbrandt, T., Peters, H., Batge, B., Brinckmann, J., and Reinhardt, D.P. (2002). Homo- and heterotypic fibrillin-1 and -2 interactions constitute the basis for the assembly of microfibrils. J. Biol. Chem. *277*, 50795–50804.
25. Singh, P., and Schwarzbauer, J.E. (2012). Fibronectin and stem cell differentiation - lessons from chondrogenesis. J. Cell Sci. *125*, 3703–3712.
26. Keene, D.R., Jordan, C.D., Reinhardt, D.P., Ridgway, C.C., Ono, R.N., Corson, G.M., Fairhurst, M., Sussman, M.D., Memoli, V.A., and Sakai, L.Y. (1997). Fibrillin-1 in human cartilage: developmental expression and formation of special banded fibers. J. Histochem. Cytochem. *45*, 1069–1082.
27. Maddox, B.K., Keene, D.R., Sakai, L.Y., Charbonneau, N.L., Morris, N.P., Ridgway, C.C., Boswell, B.A., Sussman, M.D., Horton, W.A., Bächinger, H.P., and Hecht, J.T. (1997). The fate of cartilage oligomeric matrix protein is determined by the cell type in the case of a novel mutation in pseudoachondroplasia. J. Biol. Chem. *272*, 30993–30997.
28. Hecht, J.T., Montufar-Solis, D., Decker, G., Lawler, J., Daniels, K., and Duke, P.J. (1998). Retention of cartilage oligomeric matrix protein (COMP) and cell death in redifferentiated pseudoachondroplasia chondrocytes. Matrix Biol. *17*, 625–633.
29. Hashimoto, Y., Tomiyama, T., Yamano, Y., and Mori, H. (2003). Mutation (D472Y) in the type 3 repeat domain of cartilage oligomeric matrix protein affects its early vesicle trafficking in endoplasmic reticulum and induces apoptosis. Am. J. Pathol. *163*, 101–110.
30. Sutton, V.R., Hyland, J.C., Phillips, W.A., Schlesinger, A.E., and Brill, P.W. (2005). A dominantly inherited spondylometaphyseal dysplasia with "corner fractures" and congenital scoliosis. Am. J. Med. Genet. A. *133A*, 209–212.
31. Schwarz-Linek, U., Werner, J.M., Pickford, A.R., Gurusiddappa, S., Kim, J.H., Pilka, E.S., Briggs, J.A., Gough, T.S., Höök, M., Campbell, I.D., and Potts, J.R. (2003). Pathogenic bacteria attach to human fibronectin through a tandem beta-zipper. Nature *423*, 177–181.
32. Pieper, U., Webb, B.M., Barkan, D.T., Schneidman-Duhovny, D., Schlessinger, A., Braberg, H., Yang, Z., Meng, E.C., Pettersen, E.F., Huang, C.C., et al. (2011). ModBase, a database of annotated comparative protein structure models, and associated resources. Nucleic Acids Res. *39*, D465–D474.
33. Bingham, R.J., Rudiño-Piñera, E., Meenan, N.A., Schwarz-Linek, U., Turkenburg, J.P., Höök, M., Garman, E.F., and Potts, J.R. (2008). Crystal structures of fibronectin-binding sites from Staphylococcus aureus FnBPA in complex with fibronectin domains. Proc. Natl. Acad. Sci. USA *105*, 12254–12258.
34. Emsley, P., and Cowtan, K. (2004). Coot: model-building tools for molecular graphics. Acta Crystallogr. D Biol. Crystallogr. *60*, 2126–2132.
35. Hubmacher, D., Sabatier, L., Annis, D.S., Mosher, D.F., and Reinhardt, D.P. (2011). Homocysteine modifies structural and functional properties of fibronectin and interferes with the fibronectin-fibrillin-1 interaction. Biochemistry *50*, 5322–5332.

The American Journal of Human Genetics, Volume *101*

Supplemental Data

Mutations in Fibronectin Cause a Subtype of Spondylometaphyseal Dysplasia with "Corner Fractures"

Chae Syng Lee, He Fu, Nissan Baratang, Justine Rousseau, Heena Kumra, V. Reid Sutton, Marcello Niceta, Andrea Ciolfi, Guilherme Yamamoto, Débora Bertola, Carlo L. Marcelis, Dorien Lugtenberg, Andrea Bartuli, Choel Kim, Julie Hoover-Fong, Nara Sobreira, Richard Pauli, Carlos Bacino, Deborah Krakow, Jillian Parboosingh, Patrick Yap, Ariana Kariminejad, Marie T. McDonald, Mariana I. Aracena, Ekkehart Lausch, Sheila Unger, Andrea Superti-Furga, James T. Lu, Baylor-Hopkins Center for Mendelian Genomics, Dan H. Cohn, Marco Tartaglia, Brendan H. Lee, Dieter P. Reinhardt, and Philippe M. Campeau

Figure S1. Radiographs of all individuals with FN1 mutations.

Family 1. Reproduced with publisher's permission from Sutton et al.[2]

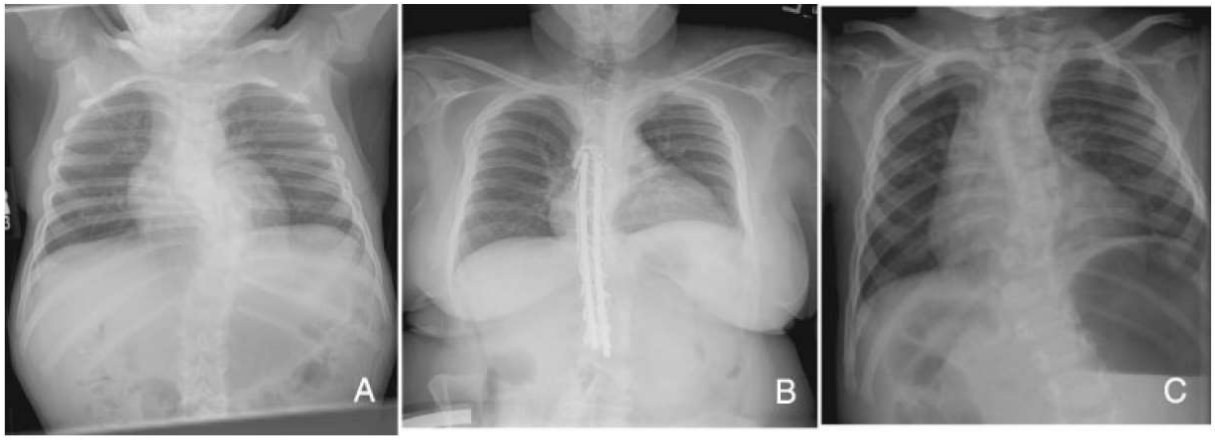

AP thoracic spine radiographs of the older boy (**A**), mother (**B**), and younger boy (**C**) showing severe scoliosis.

Lateral views of the lumbar spine. **A**: Younger boy at 3 years of age; L4 vertebral body is almost completely aplastic with only posterior elements present and L5 is hypoplastic. **B**: Older boy at 5 years of age showing hypoplasia of T12 and ovoid vertebral bodies. S1 has a triangular configuration.

A: AP pelvis and hips demonstrating absence of coxa vara in older boy. **B**: Hand image of mother demonstrating absence of brachydactyly.

Arrows in the following panels point to metaphyseal fragmentation or "corner fractures". **A**: Right knee and leg radiograph of younger boy at 3 years of age showing metaphyseal dysplasia. **B**: Proximal humerus of younger boy at 3 years of age. **C**: Right knee of older boy at 5 years of age. **D**: Right shoulder radiograph of older boy at 5 years of age showing fragmented ossification and metaphyseal dysplasia.

Family 2

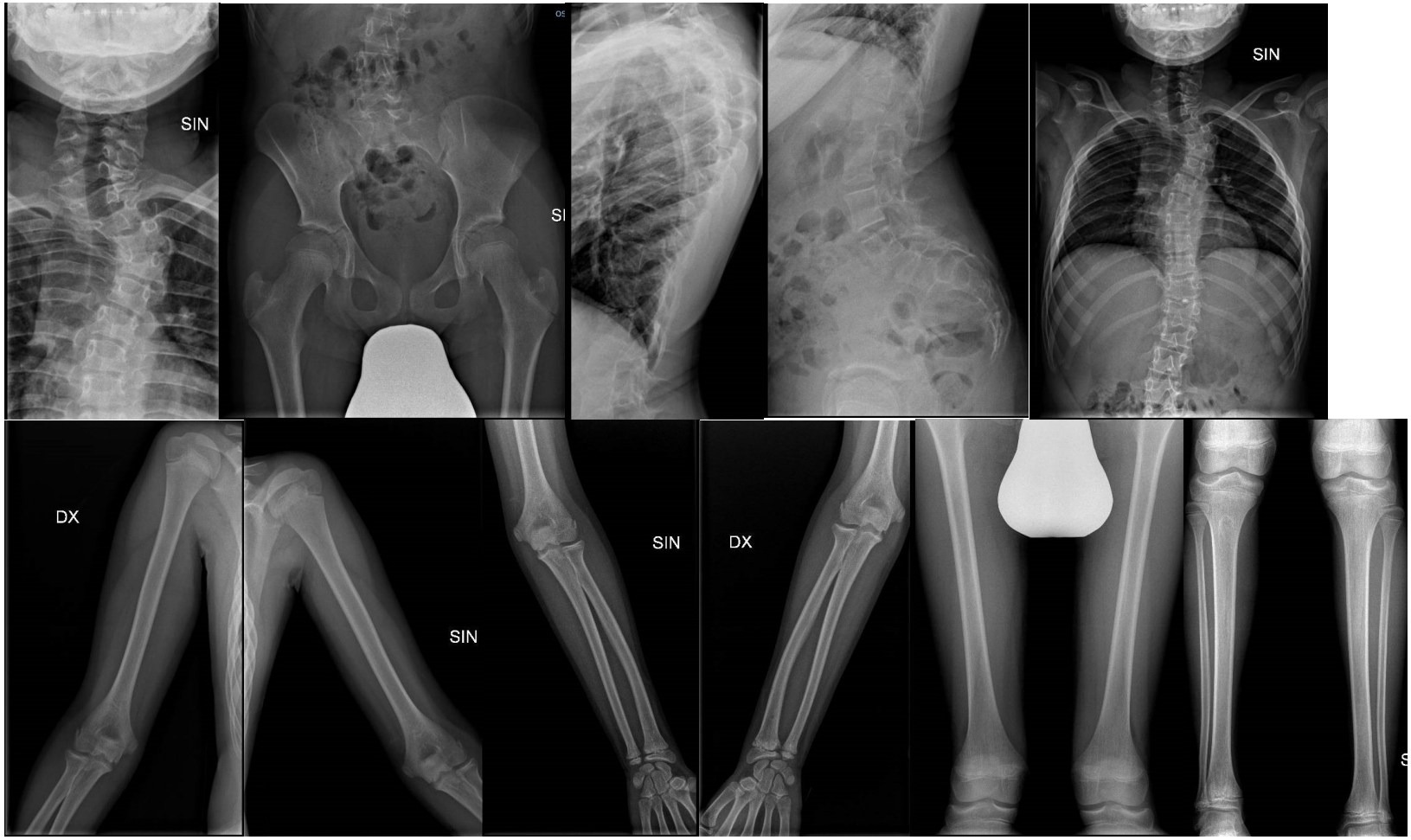
SIN
SI
SIN
DX
SIN
SIN
DX


DX
DX
S

Family 3

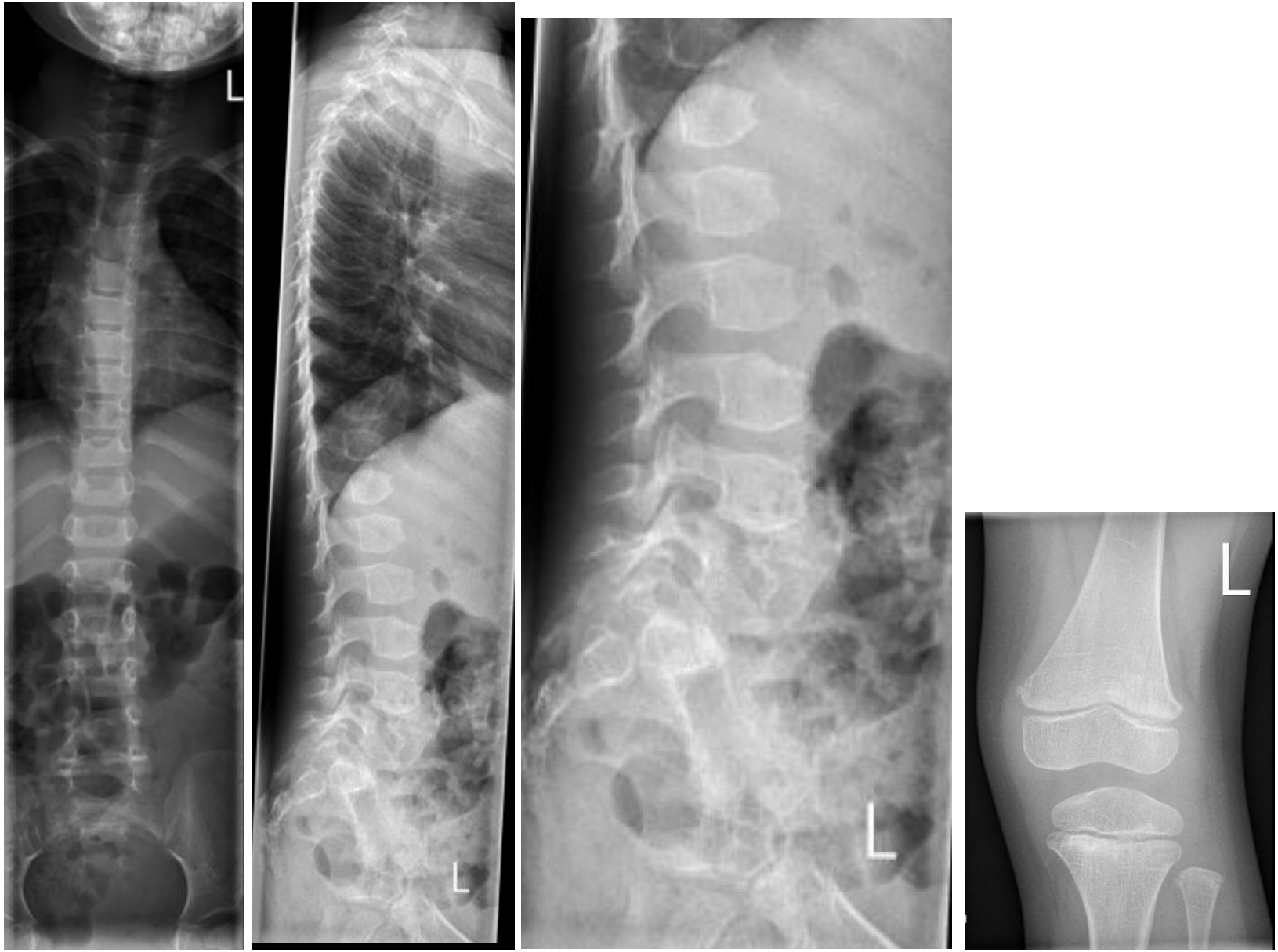
L
L
L
L




Family 4



1974

Famly 5

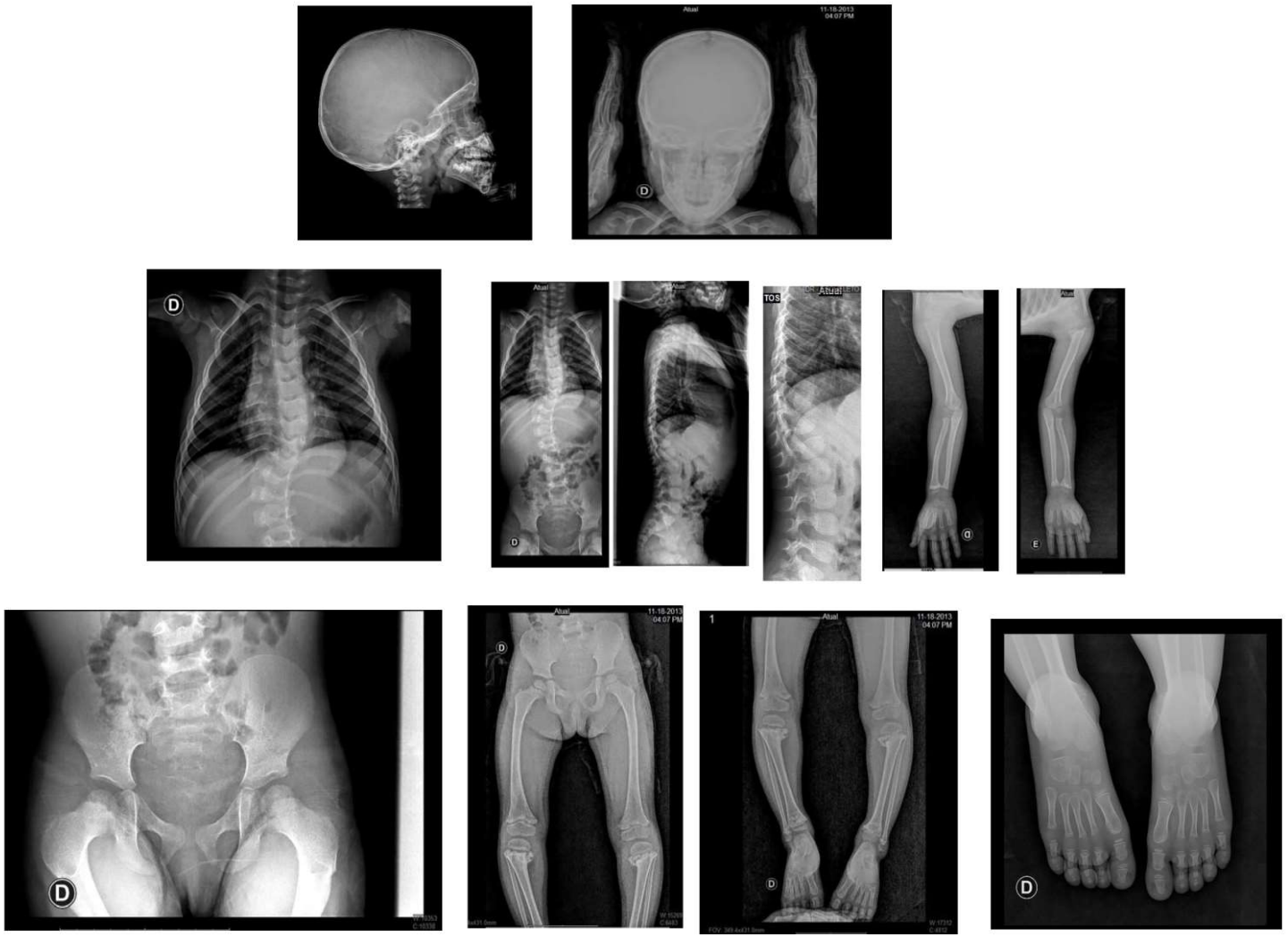


11779.3
-4439.2


Atual

Family 6

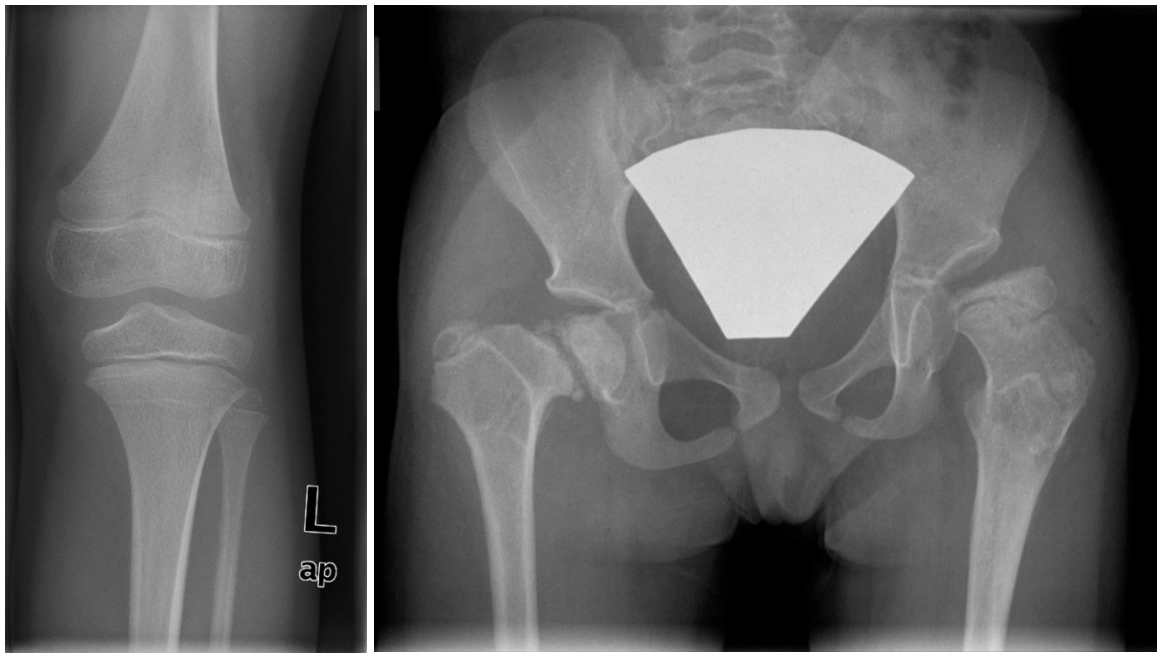

Family 7

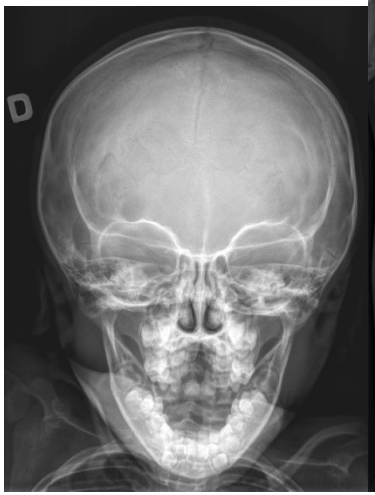

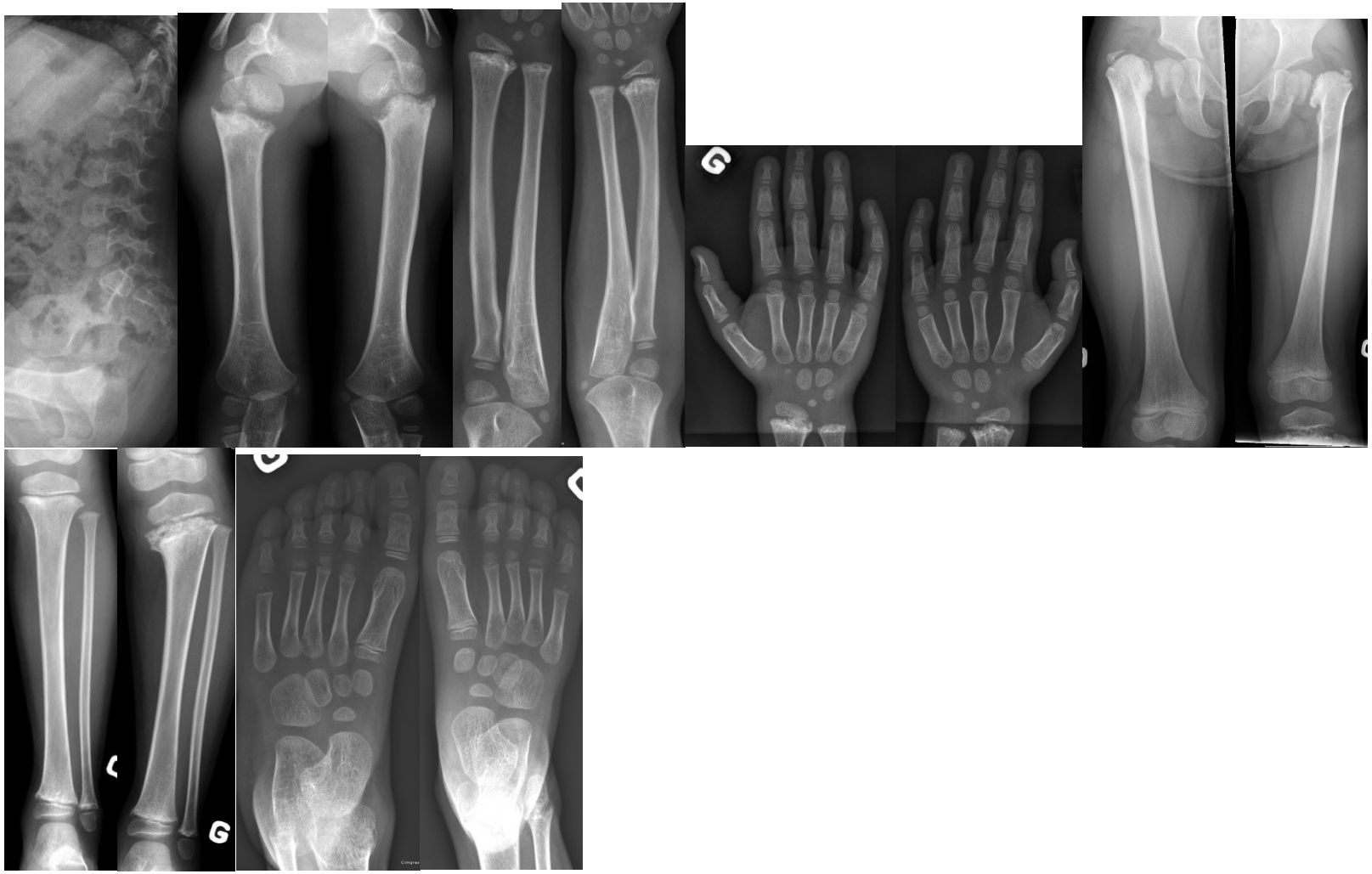

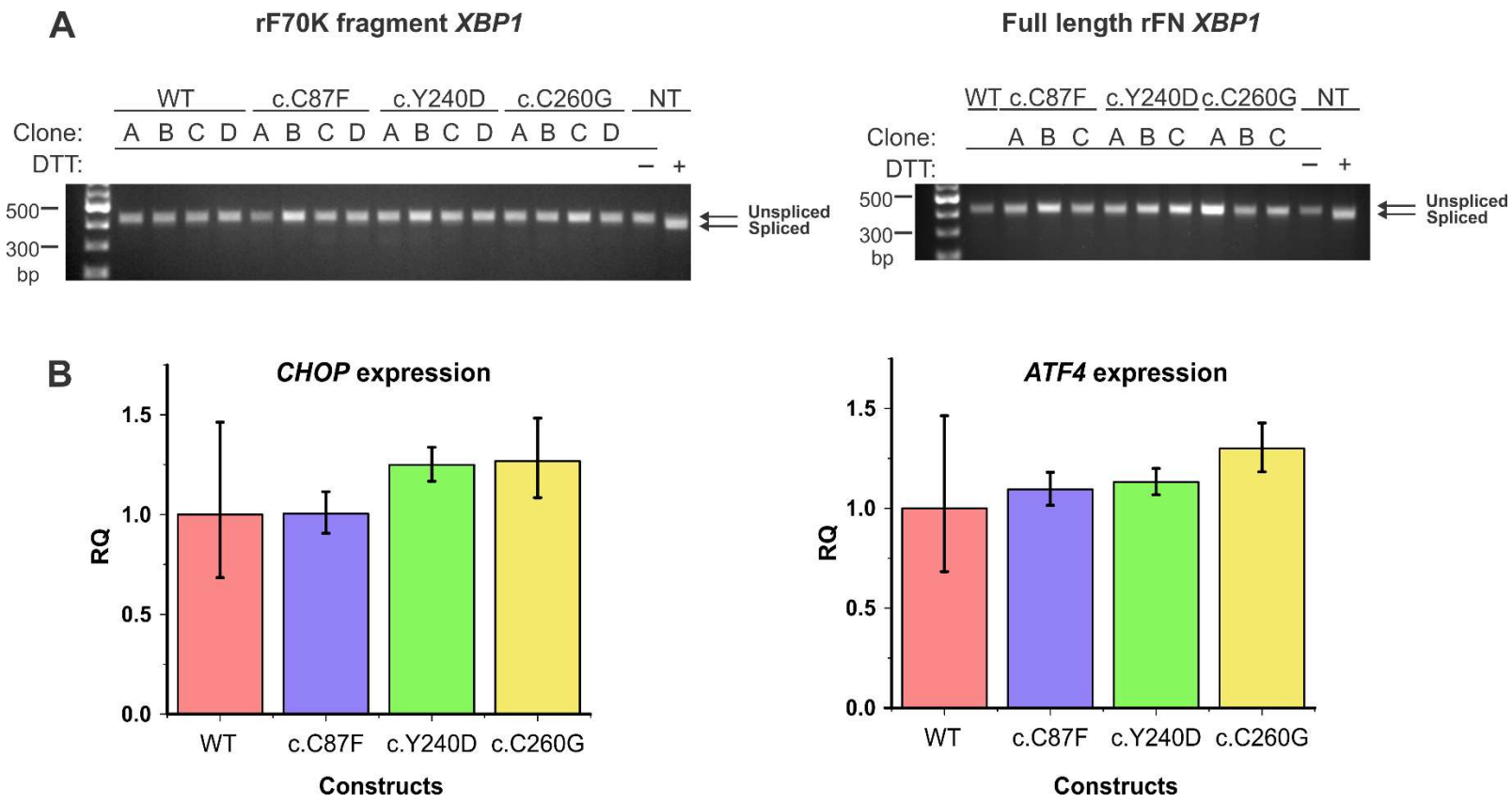

Figure S2. Analysis of the unfolded protein response of the recombinant rF70K and rFN wild-type and mutant proteins.

A) *XBP1* mRNA analysis. Mutations do not induce *XBP1*-mediated unfolded protein response. rF70K wild-type (WT) and mutants were analyzed in the left panel, and full length rFN WT and mutants in the right panel. NT represents non-transfected HEK293 cells as controls. Addition of dithiothreitol (DTT) for 1 h induces the unfolded protein response and causes *XBP1* splicing and is included as a positive control. The unspliced amplification product is 424 bp, the spliced product is 398 bp. Note that all analyzed mutations, both in rF70K and in full length rFN, do not induce the *XBP1*-mediated unfolded protein response (absence of the 398 bp band). **B**) qPCR mRNA expression analysis of *CHOP* and *ATF4* from full length rFN WT and rFN mutant cells. Both analyses showed no significant changes between rFN WT and the rFN mutants. RQ represents relative quantification of mRNA levels normalized to *GAPDH* levels. The rFN mutants were compared to the rFN WT, set to 1. Quantitative real time PCR was performed in a StepOne Real-Time PCR System (Applied Biosystems) using SYBR Select Master Mix (ThermoFisher Scientific), according to the manufacturer's protocol. Melt-curve analysis was performed after each run to determine the specificity of the detected product. Relative quantification of mRNA levels (fold change) was calculated using the $2^{-\Delta\Delta Ct}$ method. Error bars represent standard deviation. The values of all mutants were not statistically different from the wild-type ($p \geq 0.05$; Student's t-test).

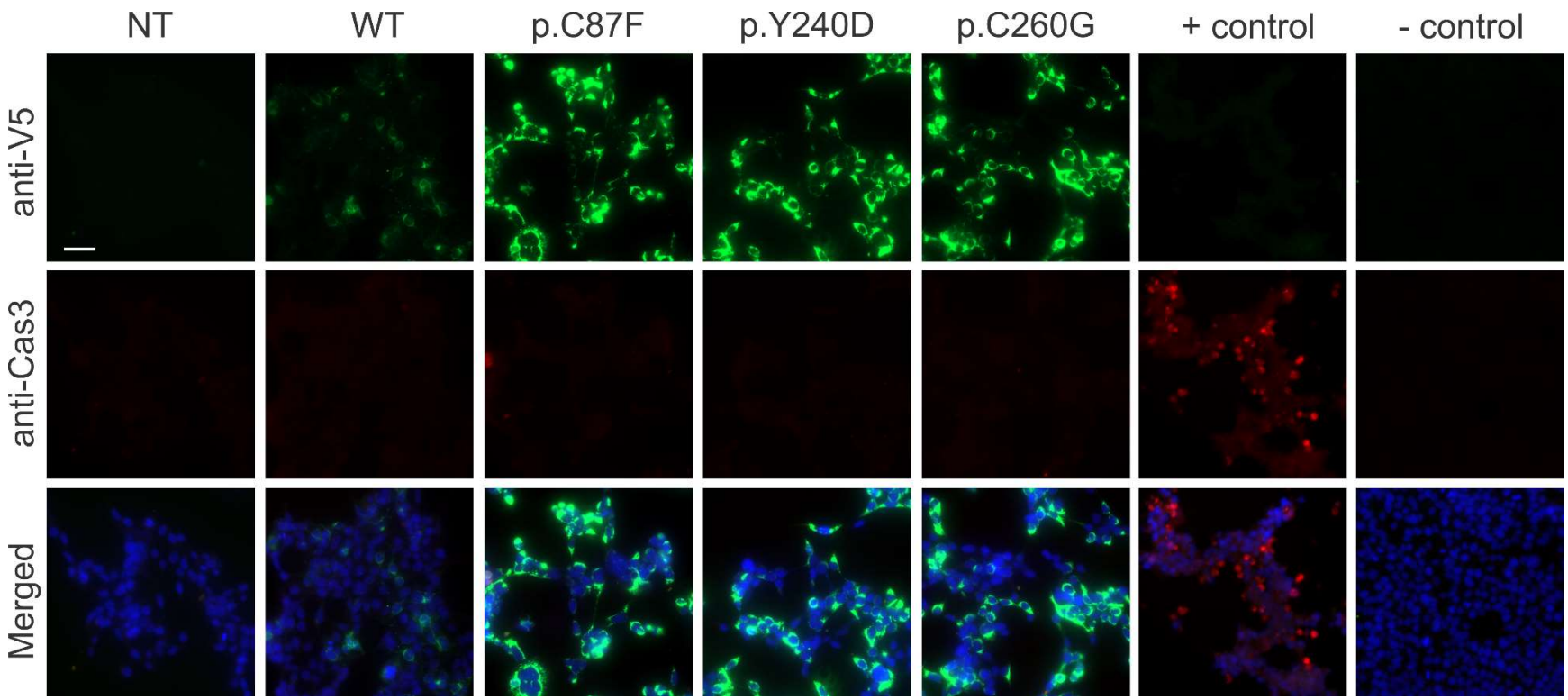

Figure S3. Analysis of caspase-3 mediated apoptosis of the recombinant rFN wild-type and mutant proteins.

Immunofluorescence of full length rFN WT and mutant cell clones with antibodies against cleaved caspase-3. Cleavage of caspase-3 is an indication of unfolded protein response mediated apoptosis. Cells were analyzed 3 days post-seeding. Note that both non-transfected HEK293 cells (NT) and transfected cells showed no staining of cleaved caspase-3 (Cas3; no red signal, primary antibody Cell Signaling; 9661S, secondary Alexa-488 conjugated antibody Thermo Fisher Scientific; A-11008), indicating the absence of detectable apoptosis. Non-transfected HEK293 cells treated for 12 h with 2µM staurosporine (Abcam; ab120056) in DMSO (0.2% DMSO final concentration) served as a positive control for apoptosis (+ control; red signal). Non-transfected HEK293 cells treated with 0.2% DMSO alone (- control) did not induce apoptosis. The rFN constructs were stained with an anti-V5 antibody (green signal). Cell nuclei were counterstained with DAPI (blue signal in the merged images). The scale bar indicates 50µm. Images were recorded at 400× magnification.

Table S1. Phenotypes of cases without a *FN1* mutation.

Family	**8[a]**	**9[a]**	**10**	**11**	**12**	**13**	**14**	**15**	**16**
Age at last assessment	12 yrs	13 yrs	4 yrs 6 mos	NA	6 yrs 6 mos	3 yrs 11 mos	1 y 4 m	5yrs 7 mos	7 yrs, 2 mos
Gender	M	M	M	F	F	F	M	F	F
Height in cm (and SD)	75.7 cm (-3 S.D,)		95.2 cm	NA	94.0 cm (ca. -4 S.D.)	99.5 cm (25th centile)	NA	unknown	101 cm (<5th centile)
Ovoid vertebral bodies	Some	Some	NA	NA	+	+	+	+	-
Other vertebral Changes (e.g. platyspondyly)	platyspondyly	platyspondyly	NA	NA	Platyspondyly ; disproportion-ate decreased height dorsally	-	-	Anterior wedging	End plate sclerosis; anterior wedging
Scoliosis	Mild	Mild	-	- (but excessive lordosis)	+ (progressive, requiring casting)	- (mild lumbar lordosis	+	unknown	+ (mild S-shaped)
Odontoid hypoplasia	+	-	NA	NA	-; but craniocervical stenosis requiring decom-pression	-	NA	-	-
Developmental coxa vara	-	+	-, slipped capital femoral epiphyses	+	-	+	+	+	+
Irregular metaphyses	+	+	NA	+	+	+	+	+	+
“Corner fractures”	+	+	+	+	+	+	+	+/-	+/-
Knee anomalies	Vara then valga	-	-	NA	Abnormal patellar tracking	Left varum	Genu varum	Dislocated patella	-

Short trunk	-	+	+	NA	-	-	-	+	unknown
Short long bones (rhizo, meso or micromelia)			-	NA	Mesomelic disproportion	-	+	(rhizo, meso	
Chest or rib anomaly (e.g. pectus)	-	-	broad	NA	AP flattening	-	NA	Short sternum	Mild anterior rib cupping
Hand and feet anomalies	-	-	-		Profound brachydactyly; short metacarpals and phalanges	-	-	-	Cupped metacarpal and phalangeal metaphyses
Other			Pes planus, hypospdias, speech delay,		Dentinogene-sis imperfecta; multiple fractures; hip uncoverage; tibia varus and internal tibial torsion	mild leg length discrepancy	relative macrocephaly, high forehead, hypertelorism, shawl scrotum, slightly bowed forearms	Unossified CFE, other epiphyses nl; metaphyseal irregularities throughout	

[a] Published (Machol K et al.[1])

Table S2. Details on targeted enrichment, sequencing and WES data analysis

Family	**1**	**2**	**3**	**4**	**5**	**6**	**7**
Connection for enrollment in project	Texas Children's bone program	Genematcher	SkelDys listserv	ISDR	Genematcher	Collaboration	Shriners Canada Skeletal Dysplasia Clinic
Site for sequencing	BCM-HGSC	OPBG	Radboud	BCM-HGSC	CEGH-CEL-Universidade de São Paulo	BGI	Calgary
Exome library capture	Roche SeqCap EZ HGSC VCRome	Illumina Nextera v1.2	No exome done, *FN1* Sanger sequencing only.	Roche SeqCap EZ HGSC VCRome	Illumina TrueSeq kit	Agilent SureSelect Human All Exon v4	Illumina TruSight One Sequencing Panel
Sequencing	Illumina HiSeq	Illumina HiSeq		Illumina HiSeq	Illumina HiSeq	Illumina HiSeq	Illumina HiSeq
Alignment	Mercury pipeline	In-house pipeline (GATK)		Mercury pipeline	Burrows-Wheeler Aligner (BWA)	Novoalign software	In-house pipeline (GATK)
Variant calling, filtering and annotation	Mercury pipeline	In-house pipeline (GATK, SnpEff, CADD/dbNSFP_SVM)		Mercury pipeline	GATK/ ANNOVAR	In-house pipeline (GATK, ANNOVAR, Perl and Bash scripts)	In-house pipeline

Supplemental References

1. Machol, K., Jain, M., Almannai, M., Orand, T., Lu, J.T., Tran, A., Chen, Y., Schlesinger, A., Gibbs, R., Bonafe, L., et al. (2017). Corner fracture type spondylometaphyseal dysplasia: Overlap with type II collagenopathies. Am J Med Genet A *173*, 733-739.
2. Sutton, V.R., Hyland, J.C., Phillips, W.A., Schlesinger, A.E., and Brill, P.W. (2005). A dominantly inherited spondylometaphyseal dysplasia with "corner fractures" and congenital scoliosis. Am J Med Genet A *133A*, 209-212.